Supplementary Information

Lu Huang[a,†], Yuan Qin[a,†], Kebiao Zhang[b], Zihao Ou[a], XinWen Rao[a], YuYing Wang[a], Bin Xiang[a, *], Xuefeng Zou[c, *], Yang Zhou[d, *], Hujun Shen[c, *]

[a] School of Chemistry and Chemical Engineering, Chongqing University, Chongqing 400044, PR. China

[b] National Key Laboratory ofAdvanced Chemical Power Sources, Guizhou Meiling PowerSources Co. Ltd, Zunyi,563003, China

[c] Guizhou Provincial Key Laboratory of Computational Nano-Material Science,Guizhou Education University, Guiyang 5500l8, China

[d] Analytical and Testing Center of Chongqing University, Chongqing University, Chongqing 401331, P. R. China

†These authors equally contribute to this work.

*Corresponding Author: xiangbin@cqu.edu.cn (B. Xiang), njzouxf@gznc.edu.cn (X. Zou), zhouyangyang@cqu.edu.cn (Y. Zhou), hujun.shen@hotmail.com (H. Shen)

Synthesis of anode materials:

Pre-treatment of carbon cloth: First, cut the carbon cloth into small rectangular pieces of 3cm*4cm; Secondly, it was soaked in 10 wt% $KMnO_4$ for 12h. Then, the substrate is oxidized by sonication for 60min, then continued with sonication in deionized water (DI) and then ethanol until the solution is clear, and finally, the cleaned oxidized CC is placed in an oven to dry[S1].

Preparation of CoFe nanowires/CC[S2]: 0.388 g (1.33 mmol) of $Co(NO_3)_2 \cdot 6H_2O$, 0.27 g (0.66 mmol) of $Fe(NO_3)_3 \cdot 9H_2O$, 0.186 g (5 mmol) of NH_4F and 0.6 g (10 mmol) of urea were sequentially dissolved in 40 mL of deionized water under stirring. After stirring in the chamber for 20min, quickly pour the solution into an autoclave and wash the above piece to immerse the CC substrate in the external solution. Maintain at 120 °C for 6h in an oven to synthesize CoFe nanoarrays grown on CC. After that, the CoFe nanowires/CC were removed, washed sequentially with water and ethanol, and then dried overnight in an oven at 60 °C.

Preparation of CoFe@NCTNs/CC composites: A piece of prepared CoFe NWs/CC (3*4 cm^2) was placed in two separate arks in the furnace with 3 g of cyanamide, 1.5 g of dicyandiamide and 1 g of melamine, respectively, with the cyanamide on the upstream side of the argon atmosphere. The samples were measured downstream with a flow of Ar gas with a heating ramp and heated at 400 °C for 2 hours. The temperature is then further raised to 800 °C at the same heating rate and maintained at this temperature for another 2 hours. After carbonization, the CoFe Nws arrays were converted to CoFe alloys embedded in N-doped carbon nanotube arrays and labeled as CoFe@NCNT/CC. The loading capacity is about 1.5 mg/cm^2.

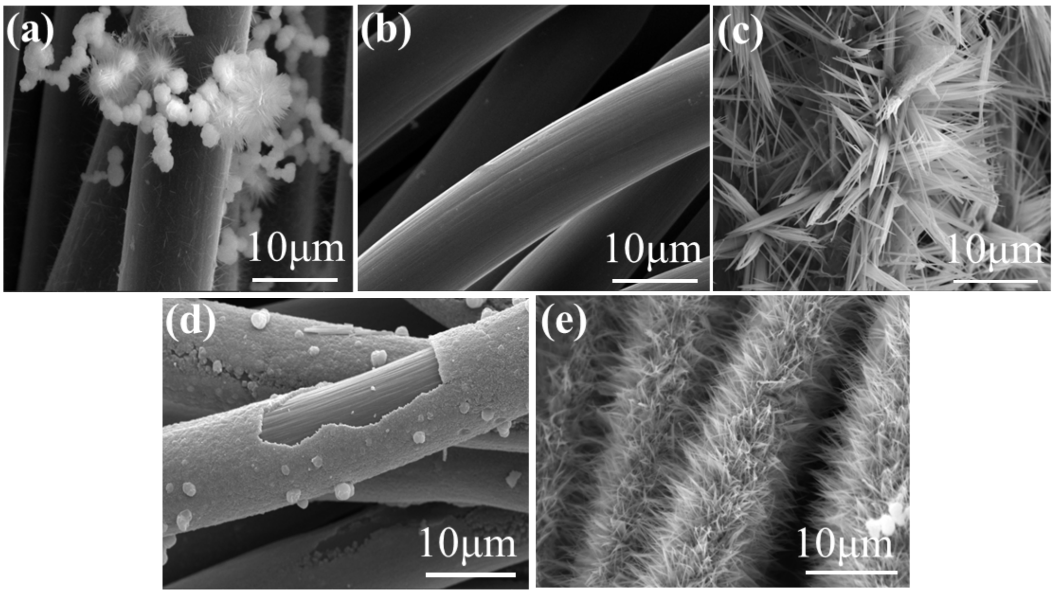

Fig. S1. Uncalcined SEM image of (a) Unactivated CC; (b) Activated CC; (c) Co; (d) Fe; and (e) CoFe

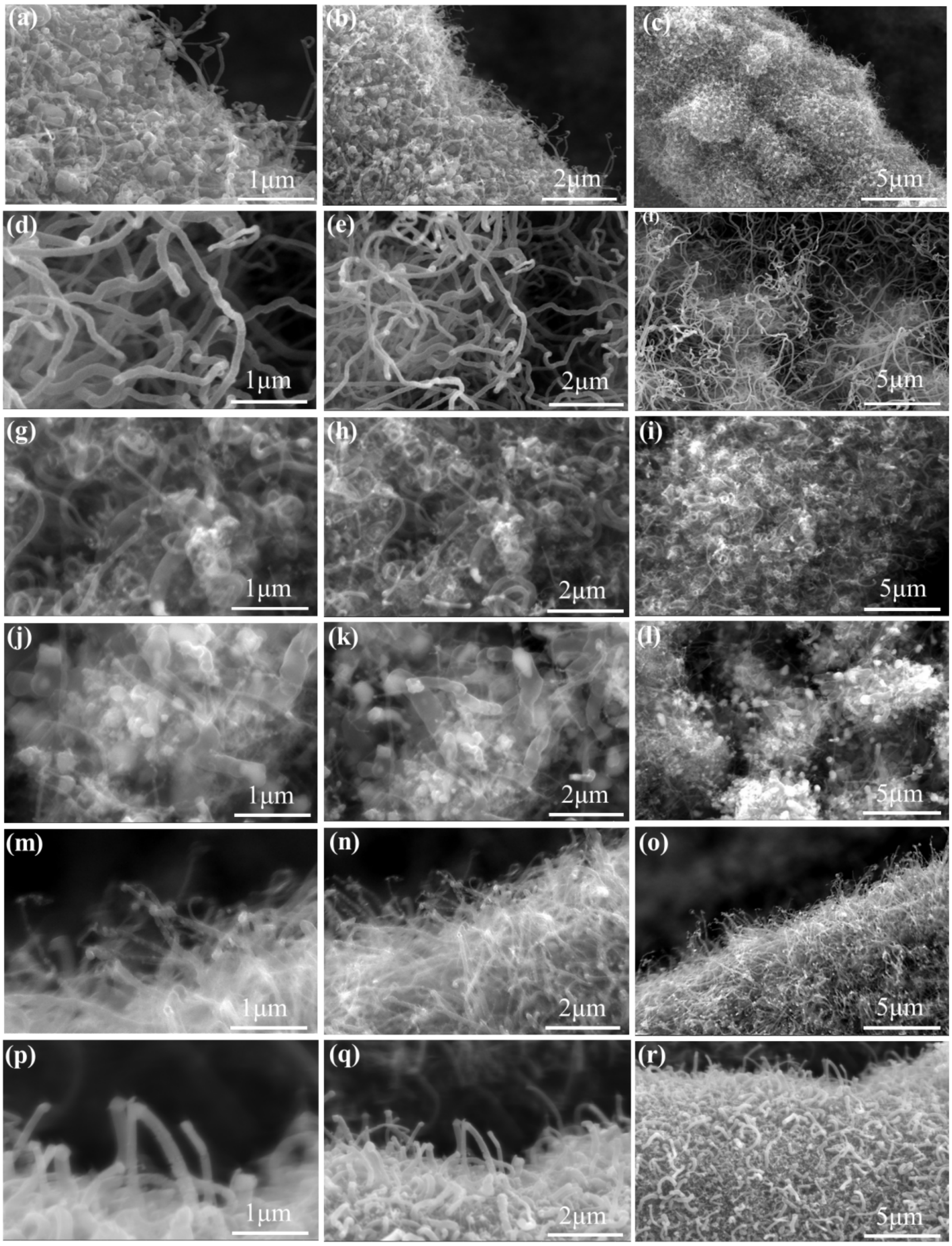

Fig. S2. The SEM image of (a, b, c) Co@NCTNs/CC; (d, e, f) Fe@NCTNs/CC; (g, h, i) 0.5:1； (j, k, l) 1:1; (m, n,o) 2:1; (p, q, r) 3:1 CoFe@NCTNs/CC

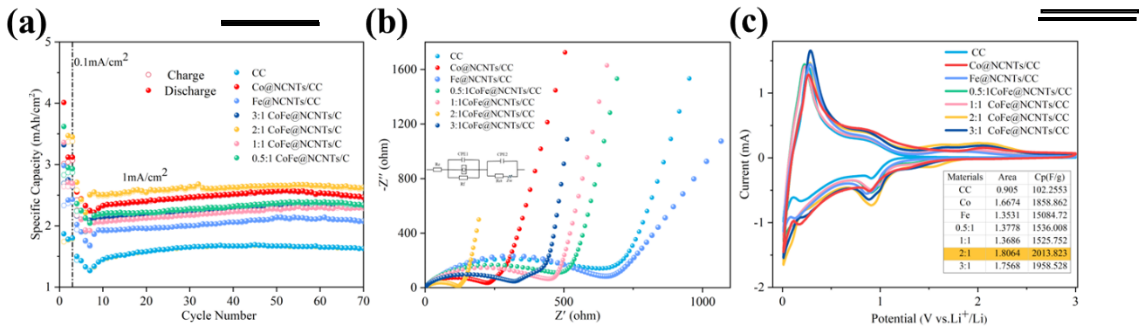

Fig. S3. The different metal complexes of (a) Nyquist plots; (b) CV curves at 0.1 $mV\cdot s^{-1}$ sweep rate; (c) Cyclic comparison at 1 $mA\cdot cm^{-2}$

Table S1. Fitting values for the impedance of different metal compounds

Samples	**Re(Ω)**	**Rf(Ω)**	**Rct(Ω)**
CC	3.075	146.5	613
Co@NCNTs/CC	3.151	234.3	246.1
Fe@NCNTs/CC	3.005	277.6	420.4
0.5:1CoFe@NCNTs/CC	2.487	7.19	547.4
1:1CoFe@NCNTs/CC	2.907	92.75	397.6
2:1CoFe@NCNTs/CC	2.435	321.4	167.9
3:1CoFe@NCNTs/CC	2.359	212.4	352.4

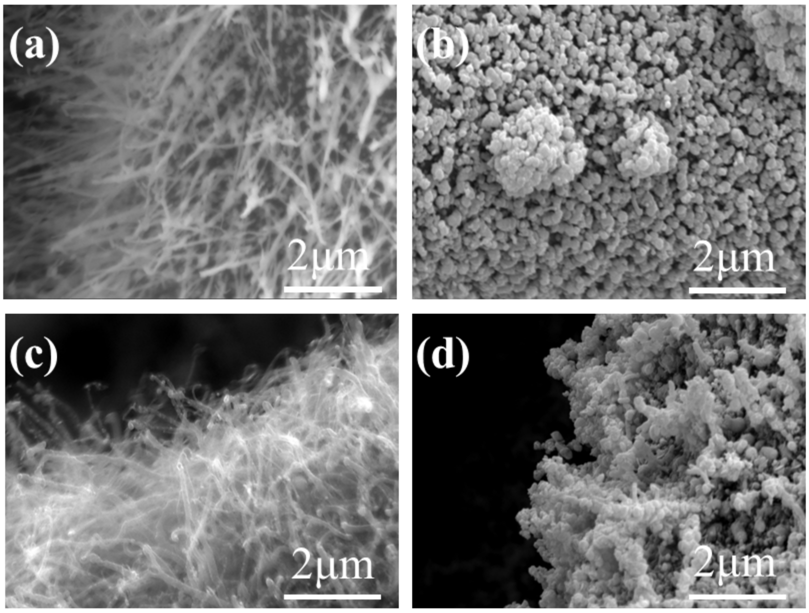

Fig. S4. The SEM plots at different calcination temperatures of (a) 400℃; (b) 700℃; (c) 800℃; (d) 900℃

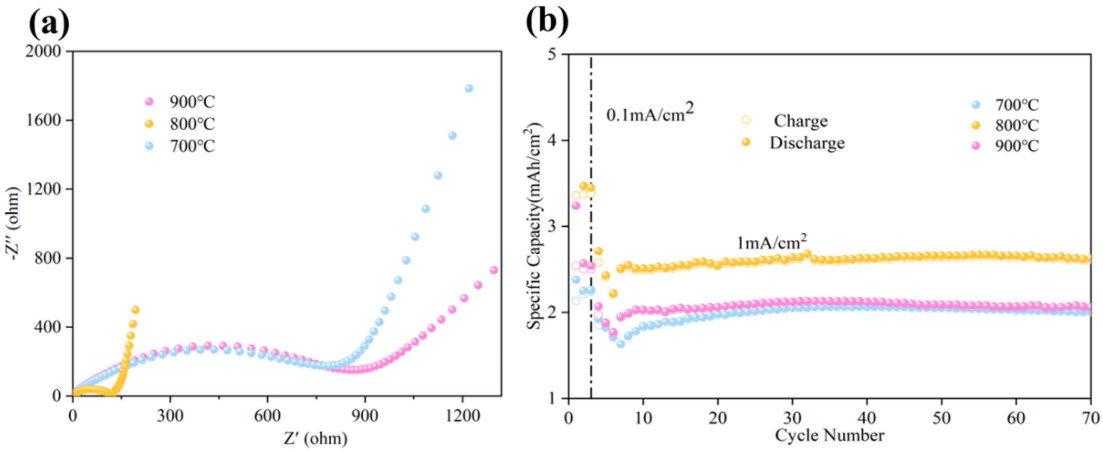

Fig. S5. The different calcination temperatures of (a) Nyquist plots; (b) Cyclic comparison at 1 $mA \cdot cm^{-2}$

Table S2. Fitting values for the impedance of different calcination temperatures

Samples (°C)	Re(Ω)	Rf(Ω)	Rct(Ω)
700	2.879	231.6	701.5
800	2.435	321.4	167.9
900	2.543	286.7	655.6

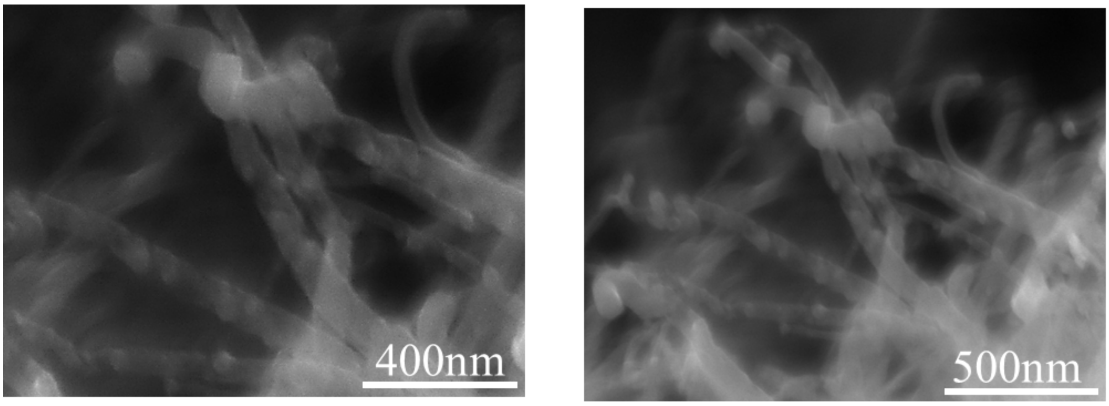

Fig. S6. The high magnification of CoFe@NCNTS/CC(DCDA)

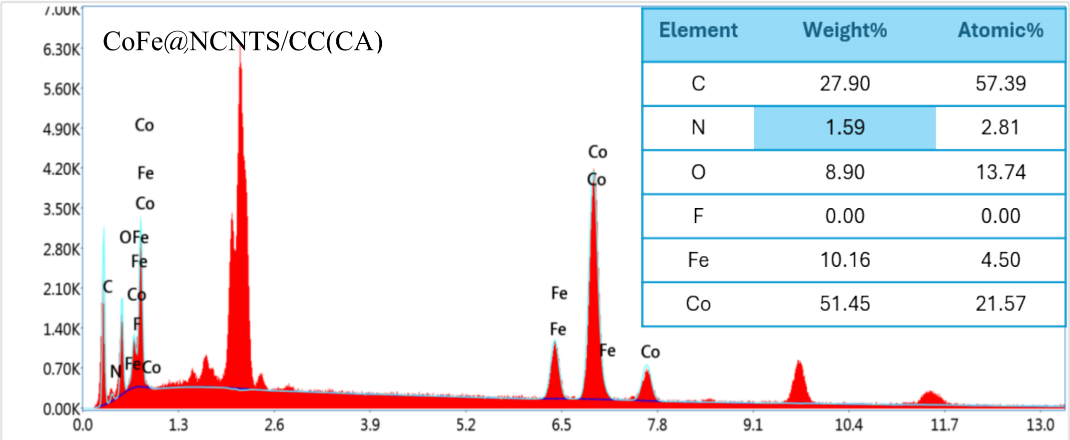

Element	Weight%	Atomic%
C	27.90	57.39
N	1.59	2.81
O	8.90	13.74
F	0.00	0.00
Fe	10.16	4.50
Co	51.45	21.57

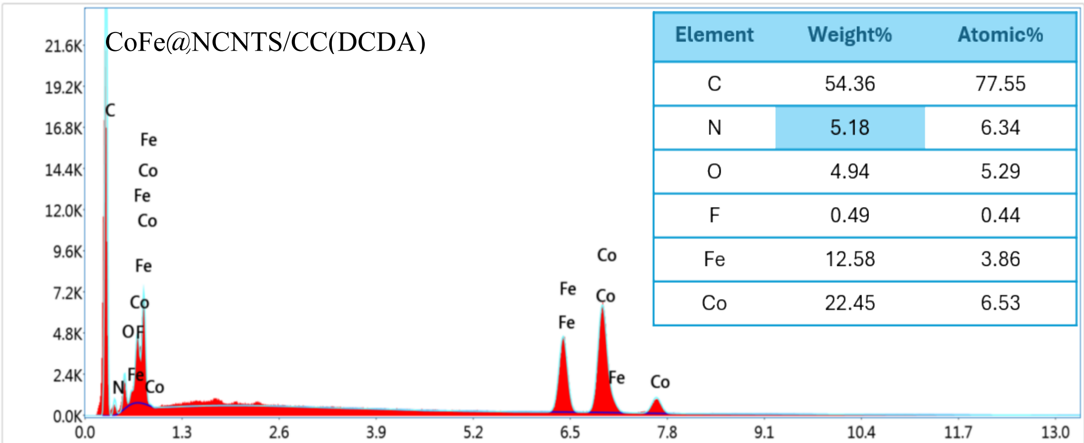

Element	Weight%	Atomic%
C	54.36	77.55
N	5.18	6.34
O	4.94	5.29
F	0.49	0.44
Fe	12.58	3.86
Co	22.45	6.53

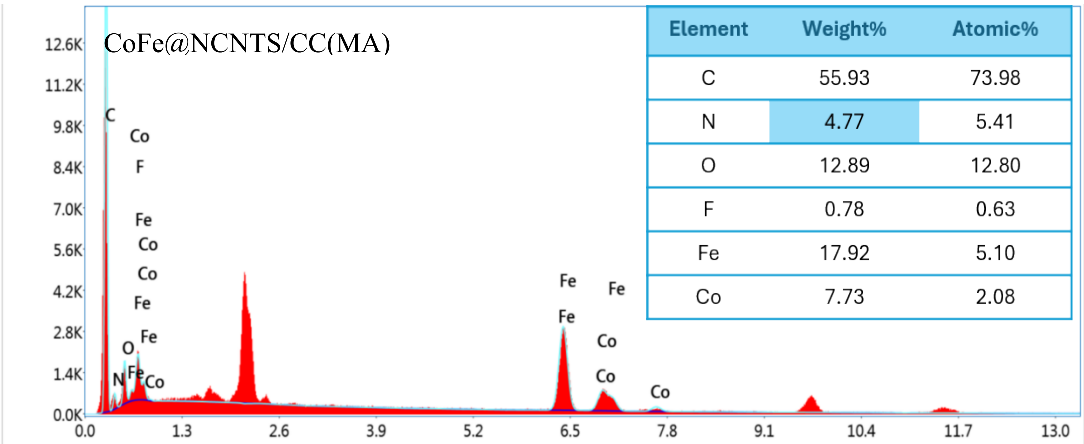

Element	Weight%	Atomic%
C	55.93	73.98
N	4.77	5.41
O	12.89	12.80
F	0.78	0.63
Fe	17.92	5.10
Co	7.73	2.08

Fig. S7. The EDS distribution of different cyanamides

Table S3. The ICP-OES Co and Fe metal distributions of different cyanamides

Sample	The concentration of Co element (mg L^{-1})	The concentration of Fe element (mg L^{-1})
CoFe@NCNTS/CC(CA)	15.8	7.2
CoFe@NCNTS/CC(DCDA)	28.6	18.6
CoFe@NCNTS/CC(MA)	26.1	13.6

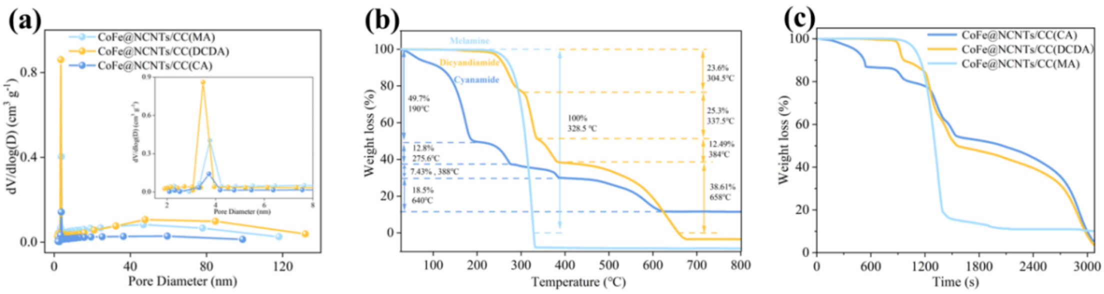

Fig. S8. (a) The pore size distributions and (b,c) TGA diagram of different cyanamide

Table S4. Fitting values for the impedance of different cyanamide conditions electrodes

Samples	**Re(Ω)**	**Rf(Ω)**	**Rct(Ω)**
CoFe@NCNTS/CC(CA)	3.301	7.568	381.4
CoFe@NCNTS/CC(DCDA)	2.435	321.4	167.9
CoFe@NCNTS/CC(MA)	2.236	194.4	178.2

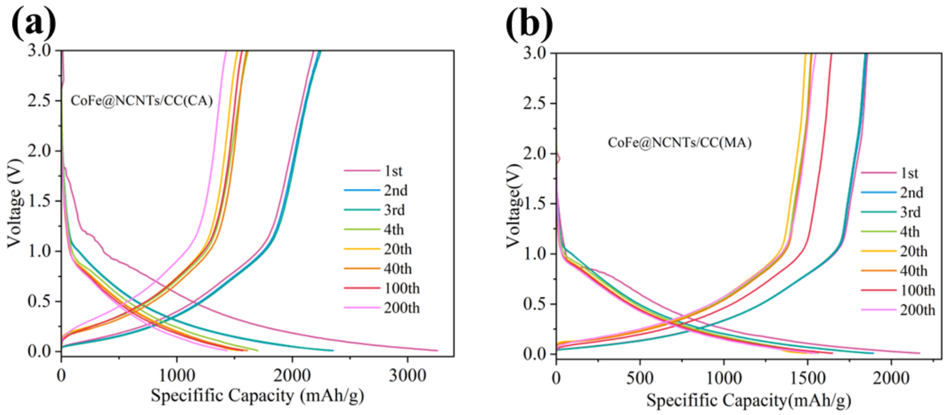

Fig. S9. The charge-discharge voltage profiles of (a) CoFe@NCNTS/CC(CA); (b) CoFe@NCNTS/CC(MA)

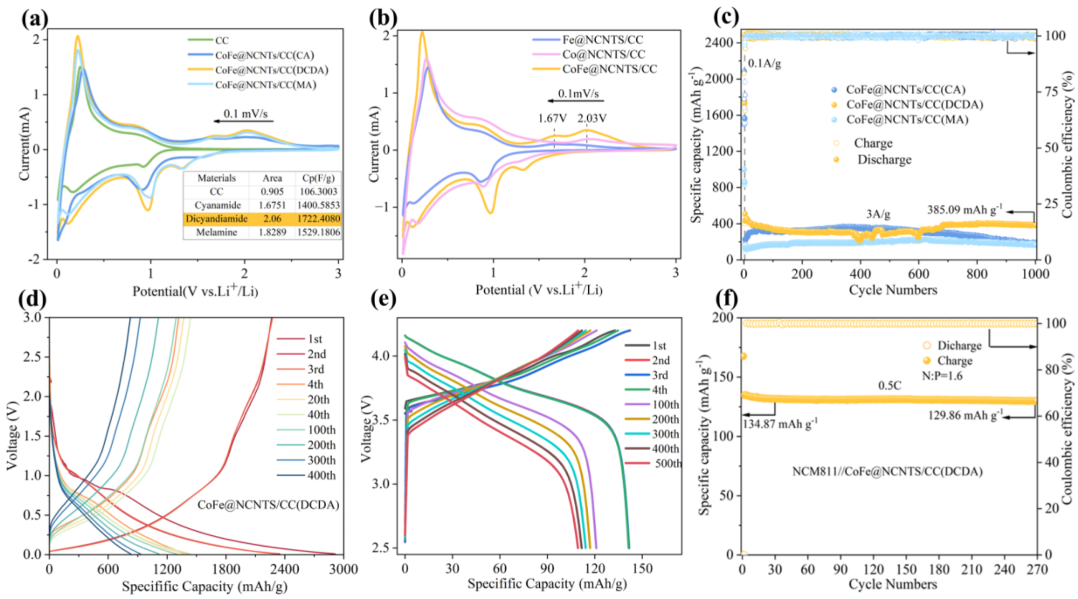

Fig. S10. (a) The CV curves of the under different cyanamide conditions electrodes at a scan rate of 0.1 mV·s^{-1} between 0.01 and 3.00 V; (b)The CV curves of the Fe@NCNTs/CC; Co@NCNTs/CC and CoFe@NCNTs/CC(DCDA) at a scan rate of 0.1 mV·s^{-1} between 0.01 and 3.00 V; (c)Cycling performances and coulombic efficiencies at 3 A·g^{-1}; (d)Galvanostatic charge-discharge curves of the CoFe@NCNTs/CC(DCDA) electrode for selected cycles at 2A g^{-1}; (e)The charge-discharge voltage curves of the full cell with CoFe@NCNTs/CC(DCDA) electrode at 1C and its cycling performance; (f) The cycle performances of CoFe@NCNTs/CC(DCDA) electrode full cells at 0.5C and Charge–discharge voltage profiles

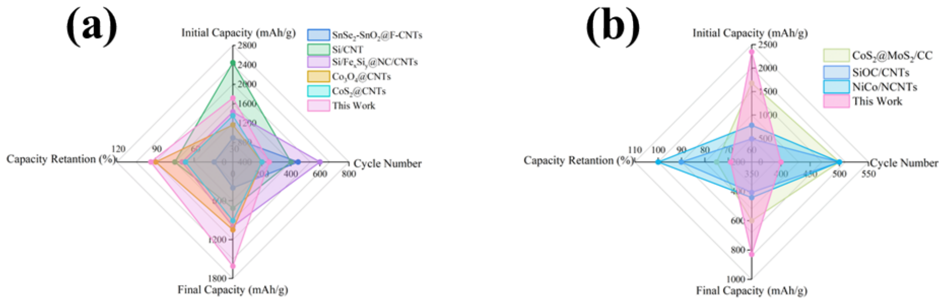

Fig. S11. Radar chart comparing the composite performance with existing carbon nanotubes under different current density conditions: (a) 1 A/g[S3-S6]; (b)2A/g[S7-S9]

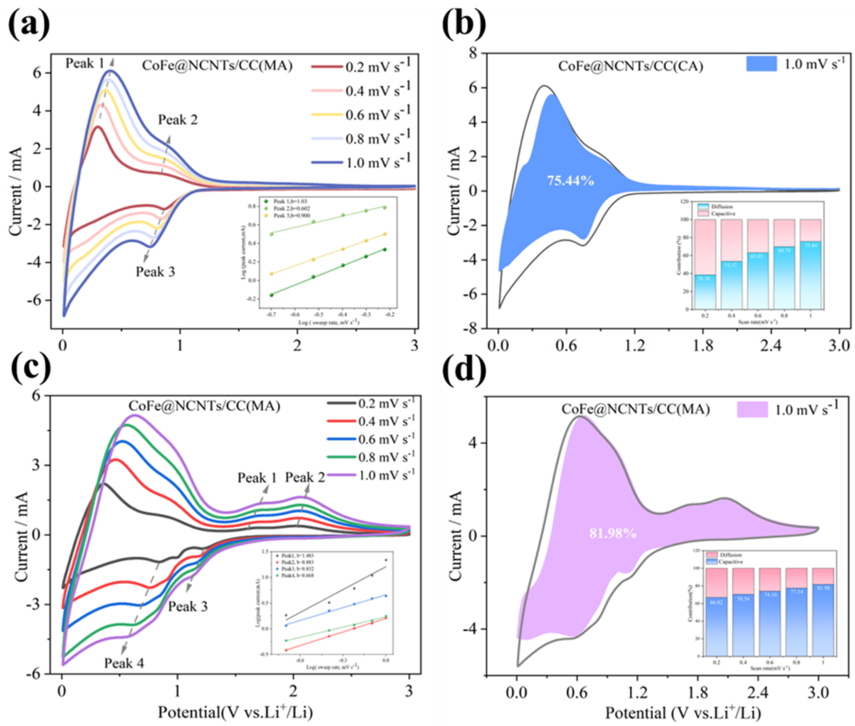

Fig. S12. (a) The CV curves of FeCo@NCNTs/CC(CA) electrode at various scan rates from 0.2 to 1.0 mV·s^{-1} and Log(i) versus Log(v) plots; (b) Capacity contribution ratios of capacitive at different scan rates of CoFe@NCNTs/CC(CA) and capacitive contribution of the electrode (blue area) at 1.0mV·s^{-1}; (c) The CV curves of FeCo@NCNTs/CC(MA) electrode at various scan rates from 0.2 to 1.0 mV·s^{-1} and Log(i) versus Log(v) plots; (d) Capacity contribution ratios of capacitive at different scan rates of CoFe@NCNTs/CC(MA) and capacitive contribution of the electrode (purple area) at 1.0mV·s^{-1}

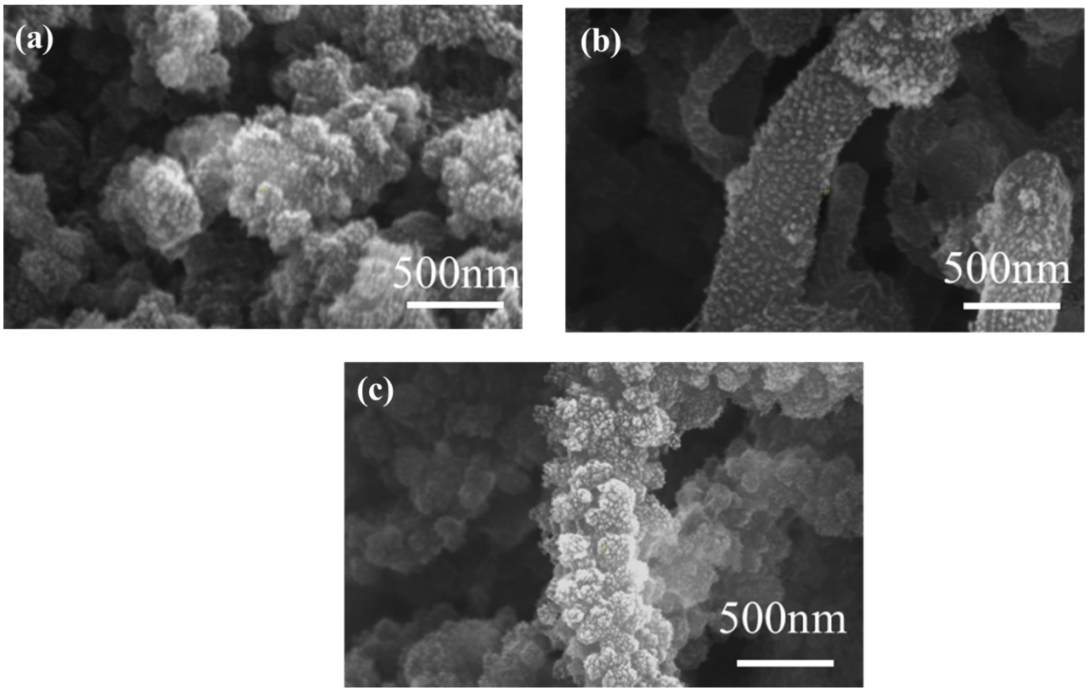

Fig. S13. Comparison of the topography of the SEM image after 1000 cycles of (a)CoFe@NCNTs/CC(CA); (b)CoFe@NCNTs/CC(DCDA)and (c)CoFe@NCNTs/CC(MA) electrode

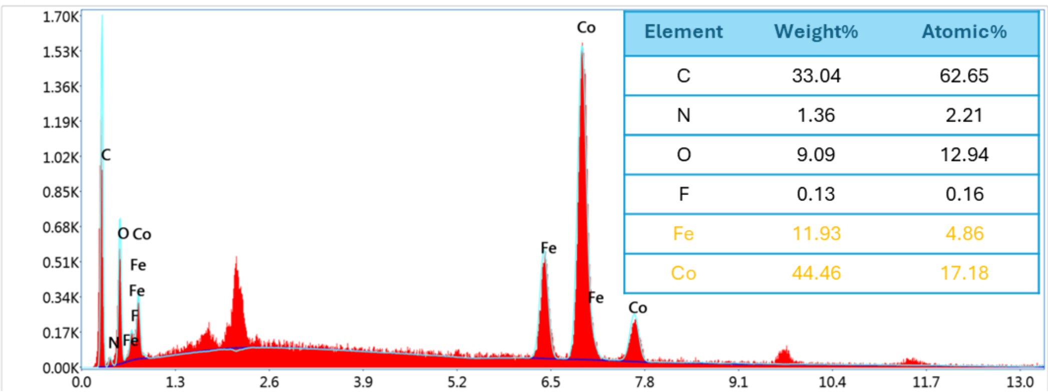

Element	Weight%	Atomic%
C	33.04	62.65
N	1.36	2.21
O	9.09	12.94
F	0.13	0.16
Fe	11.93	4.86
Co	44.46	17.18

Fig. S14. The EDS distribution of CoFe@NCNTs/CC(DCDA) after 200 cycles

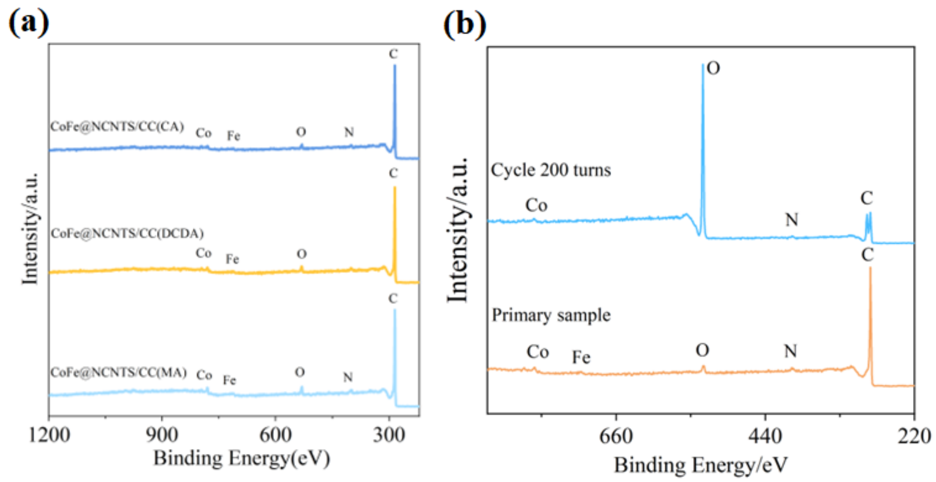

Fig. S15. (a) Full spectrum of CoFe@NCNTs/CC prepared by different cyanamide precursors; (b) Full spectrum before and after CoFe@NCNTs/CC (DCDA) cycle

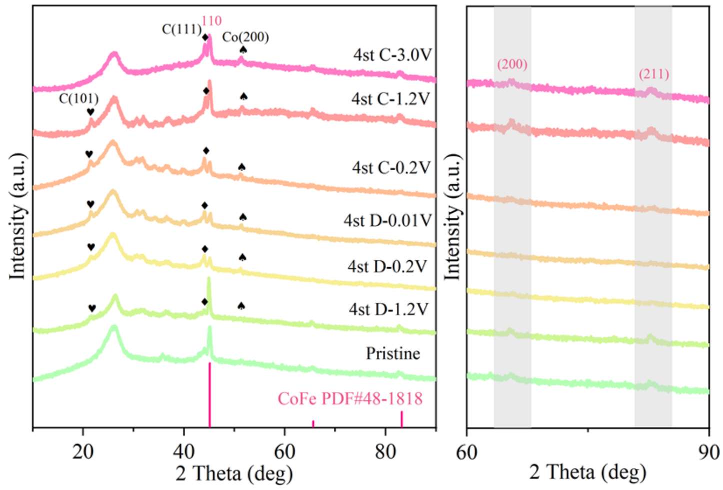

Fig. S16. In-situ XRD at different charge-discharge voltages after three cycles of activation

Table S5. In a recent report, the performance of relevant carbon nanotube materials in batteries under charge-discharge conditions is compared

S.no.	Electrodes name	Storage capacity/mAh g^{-1}	Current density	Cyclic life/no.of cycle	Ref.
1	Co_9S_8@NBNT	945	1000mA g^{-1}	2500	S10
2	CoS_2@MoS_2/CC	600	2000mA g^{-1}	500	S7
3	SiOC/CNTs	407.37	2000mA g^{-1}	1000	S11
4	SiO_x@C/MWCNT	915.89	1000mA g^{-1}	200	S12
5	NiCo/NCNTS	670.2	2000mA g^{-1}	1000	S9
6	Co_3O_4@CNTs	1037.6	1000mA g^{-1}	200	S6
7	CoS_2@CNTs	801.2			

References

S1. D. Guo, X. Yu, W. Shi, Y. Luo, Q. Li and T. Wang, Facile Synthesis of Well-Ordered Manganese Oxide Nanosheet Arrays on Carbon Cloth for High-Performance Supercapacitors, *Journal of Materials Chemistry A*, 2014, **2**, 8833-8838.

S2. J. Tian, Q. Liu, A. M. Asiri and X. Sun, Self-Supported Nanoporous Cobalt Phosphide Nanowire Arrays: An Efficient 3D Hydrogen-Evolving Cathode over the Wide Range of pH 0-14, *Journal of the American Chemical Society*, 2014, **136**, 7587-7590.

S3. H. Sun, W. Wang, L. Zeng, C. Liu, S. Liang, W. Xie, S. Gao, S. Liu and X. Wang, High-Capacity and Ultrastable Lithium Storage in $SnSe_2$-SnO_2@NC Microbelts Enabled by Heterostructures, *Dalton Transactions*, 2022, **51**, 12071-12079.

S4. R. Liu, C. Shen, Y. Dong, J. Qin, Q. Wang, J. Iocozzia, S. Zhao, K. Yuan, C. Han, B. Li and Z. Lin, Sandwich-Like CNTs/Si/C Nanotubes as High Performance Anode Materials for Lithium-Ion Batteries, *Journal of Materials Chemistry A*, 2018, **6**, 14797-14804.

S5. D. Li, M. Zhang, L. Zhang, X. Xu, Q. Pan, Y. Huang, F. Zheng, H. Wang and Q. Li, Constructing Three-Dimensional N-Doped Carbon Coating Silicon/Iron Silicide Nanoparticles Cross-Linked by Carbon Nanotubes as Advanced Anode Materials for Lithium-Ion Batteries, *Journal of Colloid and Interface Science*, 2023, **629**, 908-916.

S6. Z.-A. Li, S.-G. Wang, P.-P. Chen, J.-T. Lei, Y.-L. Hou, J.-Z. Chen and D.-L. Zhao, Interface Engineering of MOF-Derived Co_3O_4@CNT and CoS_2@CNT Anodes with Long Cycle Life and High-Rate Properties in Lithium/Sodium-Ion Batteries, *ACS Applied Materials & Interfaces*, 2024, **16**, 19730-19741.

S7. S. Du, C. Wu, L. Ao, X. Zhou, K. Jiang, L. Shang, Y. Li, J. Zhang, Z. Hu and J. Chu, Significantly Enhanced Lithium Storage by In Situ Grown CoS_2@MoS_2 Core-Shell Nanorods Anchored on Carbon Cloth, *Chemical Engineering Journal*, 2021, **420**, 127714.

S8. C. Hu, Z. Cen, Y. Quan, Q. Zhang, X. Jian, K. Liang, Y. Song and J. Xu, SiOC/CNTs Composites as Anodes for Lithium-Ion Batteries, *Chemical Engineering Journal*, 2024, **493**, 152610.

S9. M. Cao, W. Wu, R. Guo, Y. Bo, C. Gao, H. Wu, M. Wang, W. Yu, J. Li, X. Liu and J. Zhang, NiCo Nanoparticles Encapsulated in Nitrogen-Doped Carbon Tubes as Anode Materials for High-Performance Lithium-Ion Batteries, *ACS Sustainable Chemistry & Engineering*, 2024, **12**, 10880-10891.

S10. Y. Zhou, Y. Zhu, B. Xu, X. Zhang, K. A. Al-Ghanim and S. Mahboob, Cobalt Sulfide Confined in N-Doped Porous Branched Carbon Nanotubes for Lithium-Ion Batteries, *Nano-Micro Letters*, 2019, **11**, 29.

S11. C. Zheng, X. Li, J. Yu, Z. Huang, M. Li, X. Hu and Y. Li, Biomass-derived lightweight SiC aerogels for superior thermal insulation, *Nanoscale*, 2024, **16**, 4600-4608.

S12. Z. W. Jianglong Wu, Chenyu Wang, Yan Wang, Hongjun Li, Hui Luo, Hao Li, Fuqiang Wang, Dianjun Li, Jinhui Yang, Research Progress on the Synthesis of Nitrogen-Containing Compounds with Cyanamide as a Building Block, *Chinese Journal of Organic Chemistry*, 2023, **43**, 436-454.